ELSEVIER

International Journal of Solids and Structures 41 (2004) 1725–1738

INTERNATIONAL JOURNAL OF SOLIDS and STRUCTURES

www.elsevier.com/locate/ijsolstr

Analysis of the localization of deformation and the complete stress–strain relation for mesoscopic heterogeneous brittle rock under dynamic uniaxial tensile loading

Xiao-ping Zhou *

School of Civil Engineering, Chongqing University, Chongqing 400045, PR China
School of Civil Engineering and Mechanics, Shanghai Jiaotong University, Shanghai 200030, PR China

Received 28 September 2002; received in revised form 30 July 2003

Abstract

Stress redistribution induced by excavation results in the tensile zone in parts of the surrounding rock mass. It is significant to analyze the localization of deformation and damage, and to study the complete stress–strain relation for mesoscopic heterogeneous rock under dynamic uniaxial tensile loading. On the basis of micromechanics, the complete stress–strain relation including linear elasticity, nonlinear hardening, rapid stress drop and strain softening is obtained. The behaviors of rapid stress drop and strain softening are due to localization of deformation and damage. The constitutive model, which analyze localization of deformation and damage, is distinct from the conventional model. Theoretical predictions have shown to consistent with the experimental results.

Keywords: Dynamic uniaxial tensile loading; Mesoscopic heterogeneous rock; Micromechanics; Localization of damage and deformation; The complete stress–strain relation

1. Introduction

Stress redistribution induced by underground engineering and slope engineering excavation results in the tensile zone in parts of the surrounding rock mass. It has been observed that the ultimate failure strength of rock is rate sensitive under dynamic uniaxial tensile loading. It is of important significance to investigate the localization of deformation, and to study the complete stress–strain relation for mesoscopic heterogeneous rock under dynamic tensile loading.

Efforts have been made to study the mechanism governing the rate-dependent behavior of rock material under dynamic tensile loading. These researches on constitutive relation are mostly based on the

* Address: School of Civil Engineering and Mechanics, Shanghai Jiaotong University, Shanghai 200030, PR China. Tel.: +86-23-6540-5987; fax: +86-23-6512-6168.
E-mail address: zhouxiaopinga@sina.com (X.-p. Zhou).

0020-7683/$ - see front matter © 2003 Elsevier Ltd. All rights reserved.
doi:10.1016/j.ijsolstr.2003.07.007

assumption of visco-elastic or visco-plastic model for rock material (Blanton, 1981; Chong et al., 1980; Okubo et al., 1993; Jin, 2001).

Rock material is typically inhomogeneous, containing initial defects, such as grain boundaries, microcracks and pores. Rock materials fail through fracture preceded by countless microcracks distributed over the bulk of rock and propagating under dynamic tensile loading. Since the problem is complex, up to now the problem is not solved by the micromechanical approach.

In this paper, based on the micromechanical approach proposed by Zhou (in press), the localization of deformation is analyzed and the complete stress–strain relation for mesoscopic heterogeneous rock under dynamic uniaxial tensile loading is investigated. The model leads to an overall anisotropic response due to the growth of tensile cracks. The overall damage evolution equations as well as the complete stress–strain relation in both the axial and transverse directions are obtained for rock material containing a number of randomly oriented preexisting microcracks. As an illustration, theoretical stress–strain curves of rock material under dynamic uniaxial tensile loads is given and compared with the experimental results.

2. Theoretical model

Consider a representative volume element featuring a mesoscopic length scale which is much larger than the characteristic length scale of microcrack, but smaller than the characteristic length scale of a macroscopic specimen. Establish the global coordinate system (x_1, x_2) and corresponding local coordinate system (x_1', x_2'), in which x_2'-axis is parallel to the normal vector **n**. It is assumed that the preexisting microcrack sizes randomly vary within the range $(2c_0, 2c_1)$, its normal forms an angle θ with respect to x_2-axis as depicted in Fig. 1.

Under static uniaxial tensile loading, the stress intensity factors at the crack tip take the following form:

$$K_I = \sigma_2 \cos^2\theta\sqrt{\pi c}, \tag{1}$$

where K_I is the mode I stress intensity factors.

The criterion of microcrack growth under static uniaxial tensile loading in a stable fashion is

$$K_I = K_{IC} \tag{2}$$

in which K_{IC} is the mode I critical stress intensity factor at weak plane under static tensile loading.

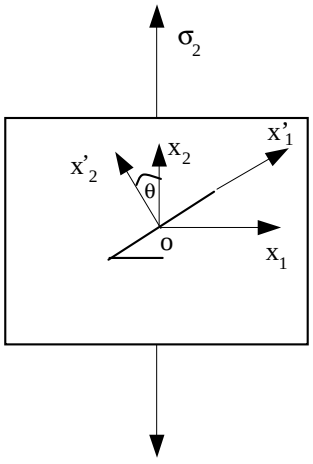

Fig. 1. Crack-weakened rock subjected to uniaxial tensile loading.

Under dynamic loads, crack growth velocities have a great influence on the dynamic SIF. In most cases, the dynamic SIF can be expressed as (Freund, 1973, 1990)

$$K_{\mathrm{ID}} = k(v)K_I, \tag{3}$$

where K_{ID} is the dynamic SIF, K_{I} is the static SIF, $k(v)$ is a function of crack growth velocity (v). The function $k(v) = 1.0$ when $v = 0$, and $k(v) = 0$ when v reaches the critical velocity of the crack growth, which is normally regarded as the velocity of a Rayleigh wave in the rock material.

The crack instability condition under dynamic loads is written as

$$K_{\mathrm{ID}} = K_{\mathrm{IC}}^{\mathrm{d}}, \tag{4}$$

where $K_{\mathrm{IC}}^{\mathrm{d}}$ is the mode I critical stress intensity factor at weak plane under dynamic tensile loading, K_{ID} is the mode I dynamic SIF.

The mode I dynamic stress intensity factor, for two-dimension in-plane crack growth, has been established by Freund (1990). The dynamic stress intensity factor may be estimated by multiplying the equivalent static stress intensity factor by an approximate formulation of $k(v)$ for brittle material (Freund, 1973, 1990):

$$k(v) = \frac{v_{\mathrm{r}} - v}{v_{\mathrm{r}} - 0.5v} \tag{5}$$

when the tensile crack is loaded by only far field uniform stress, where v_{r} is the velocity of Rayleigh wave, $v = (\mathrm{d}l/\mathrm{d}t)$.

Substituting (1) and (5) into (3), the mode I dynamic stress intensity factor can be written as

$$K_{\mathrm{ID}} = \frac{v_{\mathrm{r}} - v}{v_{\mathrm{r}} - 0.5v}\sigma_2 \cos^2\theta\sqrt{\pi c}. \tag{6}$$

Substitution of (6) into (4), we have

$$\sigma_2 = \frac{K_{\mathrm{IC}}^{\mathrm{d}}(v_{\mathrm{r}} - 0.5v)}{(v_{\mathrm{r}} - v)\cos^2\theta\sqrt{\pi c}}, \tag{7}$$

where $K_{\mathrm{IC}}^{\mathrm{d}}$ is the mode I critical stress intensity factor at weak plane under dynamic tensile loading.

From (7), it is clear that the first microcrack to become unstable is oriented along $\theta = 0$ direction and with maximum initial size c_1, the corresponding threshold load is defined as

$$\sigma_{2c} = \frac{K_{\mathrm{IC}}^{\mathrm{d}}(v_{\mathrm{r}} - 0.5v)}{(v_{\mathrm{r}} - v)\sqrt{\pi c_1}}. \tag{8}$$

Since microcrack sizes randomly vary within the range $(2c_0, 2c_1)$, the maximum and minimum microcrack size c_1 and c_0 should be used in (7) instead of c in order to determine the critical domain of unstable microcrack growth. Therefore, (6) and (7) can determine the maximum angle, θ_{u1}, at which microcracks with maximum initial size c_1 become unstable. Similarly, the minimum angle, θ_{u0}, can be determined, at which all microcracks become unstable.

$$\theta_{u1} = \arccos\left[\frac{(v_{\mathrm{r}} - 0.5v)K_{\mathrm{IC}}^{\mathrm{d}}}{(v_{\mathrm{r}} - v)\sigma_2\sqrt{\pi c_1}}\right]^{1/2}, \qquad \theta_{u0} = \arccos\left[\frac{(v_{\mathrm{r}} - 0.5v)K_{\mathrm{IC}}^{\mathrm{d}}}{(v_{\mathrm{r}} - v)\sigma_2\sqrt{\pi c_0}}\right]^{1/2}. \tag{9}$$

In addition, at a specified microcrack orientation θ within the range $(\theta_{u0}, \theta_{u1})$, the minimum microcrack size required to activate mode I growth can be evaluated from (7)

$$c_{01} = \frac{(v_{\mathrm{r}} - 0.5v)^2(K_{\mathrm{IC}}^{\mathrm{d}})^2}{(v_{\mathrm{r}} - v)^2\sigma_2^2\pi\cos^4\theta}. \tag{10}$$

If $0 < \sigma_2 < \sigma_{2c}$, that is, the stage of linear elasticity, no microcrack growth begins. The compliance tensor attributable to a single open crack is given by (Sumarac and Krajcinovic, 1987)

$$S_{ij} = \frac{2\pi c^2(1-v_0^2)}{A_0 E_0}(g_{2i}g_{2j} + g_{3i}g_{3j}), \tag{11}$$

where A_0 is the representative element area of rock material, E_0 is Young's modulus, v_0 is Poisson's ratio, $\boldsymbol{g}_{ij}$ are the components of the transformation matrix between the two coordinate system:

$$[g] = \begin{bmatrix} \cos^2\theta & \sin^2\theta & \sin 2\theta \\ \sin^2\theta & \cos^2\theta & -\sin 2\theta \\ -\frac{\sin 2\theta}{2} & \frac{\sin 2\theta}{2} & \cos 2\theta \end{bmatrix}.$$

The inelastic compliance tensor due to all preexisting open microcracks with the original sizes can be evaluated by

$$S_{ij}^{i1} = \frac{(1-v_0^2)}{E_0}\rho \int_0^{\frac{\pi}{2}}\int_{c_0}^{c_1}(g_{2i}g_{2j} + g_{3i}g_{3j})p(c)p(\theta)c^2\,\mathrm{d}c\,\mathrm{d}\theta, \tag{12}$$

where $\rho = N/A_0$ and N is the number of microcracks, A_0 is the representative element area of rock material, $p(\theta)$ and $p(c)$ are the probability density function describing the distribution of orientations and sizes of microcracks in rock material, respectively. E_0 is Young's modulus, v_0 is Poisson's ratio.

The overall effective compliance tensor can be obtained as

$$S_{ij} = S_{ij}^0 + S_{ij}^{i1} \tag{13}$$

in which S_{ij}^0 is the elastic and isotropic compliance of an undamaged rock material with Young's modulus E_0 and Poisson's ratio v_0.

During the stage of linear elasticity, the stress–strain relation takes the following form:

$$\varepsilon_{ij} = (S_{ij}^0 + S_{ij}^{i1})\sigma_{ij}. \tag{14}$$

If $\sigma_2 = \sigma_{2c}$, the microcracks in the plane $\theta = 0$ with maximum initial size $2c_1$ become unstable and increase in size until reaching maximum characteristic length $2c_2$.

If $\sigma_{2c} \leqslant \sigma_2 < \sigma_{2cc}$ (σ_{2cc} is ultimate strength of rock material), that is, the stage of prepeak nonlinear hardening, more microcracks become activated, the compliance tensor contributing from stable and unstable microcracks, S_{ij}^{i1}, S_{ij}^{i2} can be computed as follows, respectively:

$$\begin{aligned} S_{ij}^{i1} = {} & \frac{(1-v_0^2)}{E_0}\rho \int_{\theta_{u1}}^{\frac{\pi}{2}}\int_{c_0}^{c_1}(g_{2i}g_{2j} + g_{3i}g_{3j})c^2p(c)p(\theta)\,\mathrm{d}c\,\mathrm{d}\theta \\ & + \frac{(1-v_0^2)}{E_0}\rho \int_{\theta_{uo}}^{\theta_{u1}}\int_{c_0}^{c_{01}}(g_{2i}g_{2j} + g_{3i}g_{3j})c^2p(c)p(\theta)\,\mathrm{d}c\,\mathrm{d}\theta, \end{aligned} \tag{15}$$

$$\begin{aligned} S_{ij}^{i2} = {} & \frac{(1-v_0^2)}{E_0}\rho \int_0^{\theta_{u0}}\int_{c_0}^{c_2}(g_{2i}g_{2j} + g_{3i}g_{3j})c^2p(c)p(\theta)\,\mathrm{d}c\,\mathrm{d}\theta \\ & + \frac{(1-v_0^2)}{E_0}\rho \int_{\theta_{u0}}^{\theta_{u1}}\int_{c_{01}}^{c_2}(g_{2i}g_{2j} + g_{3i}g_{3j})c^2p(c)p(\theta)\,\mathrm{d}c\,\mathrm{d}\theta, \end{aligned} \tag{16}$$

where

$$\theta_{u1} = \arccos\left[\frac{(v_r - 0.5v)K_{IC}^d}{(v_r - v)\sigma_2\sqrt{\pi c_1}}\right]^{1/2}, \qquad \theta_{u0} = \arccos\left[\frac{(v_r - 0.5v)K_{IC}^d}{(v_r - v)\sigma_2\sqrt{\pi c_0}}\right]^{1/2},$$

$$c_{01} = \frac{(v_r - 0.5v)^2 (K_{IC}^d)^2}{(v_r - v)^2 \sigma_2^2 \pi \cos^4 \theta}.$$

The overall effective compliance tensor can be expressed as

$$S_{ij} = S_{ij}^0 + S_{ij}^{i1} + S_{ij}^{i2}. \tag{17}$$

During the stage of prepeak nonlinear elasticity, the stress–strain relation can be written as

$$\varepsilon_{ij} = (S_{ij}^0 + S_{ij}^{i1} + S_{ij}^{i2})\sigma_{ij}. \tag{18}$$

Under high stress, some microcrack arrested by the energy barriers, like grain boundaries, will satisfy the second growth criterion and propagate in an unstable fashion, causing localization of deformation and damage. The second growth criterion under dynamic uniaxial tensile loading can be written as

$$K_{ID} = K_{ICC}^d, \tag{19}$$

where K_{ICC}^d is the critical value of SIF describing the resistance of rock material against microcrack growth under dynamic loading.

According to (6) and (19), it is clear that the first microcrack to become unstable are oriented along $\theta = 0$ direction and with maximum characteristic size c_2, the corresponding peak load is defined as

$$\sigma_{2cc} = \frac{(v_r - 0.5v)K_{ICC}^d}{(v_r - v)\sqrt{\pi c_2}}. \tag{20}$$

If $\sigma_2 < \sigma_{2cc}$, no microcrack propagates in an unstable fashion.

If $\sigma_2 = \sigma_{2cc}$, that is, the stage of rapid stress drop, some microcracks nearly normal to the tension direction and with maximum characteristic size c_2 propagate in an unstable fashion. As mentioned above, the distribution of sizes and orientations of microcracks in rock material can be described by the probability density function $p(c)$ and $p(\theta)$, respectively. If the number of microcracks normal to tensile direction is zero, it is assumed that microcracks whose orientations are within a small orientation scope $0 \leqslant \theta \leqslant \theta_{cc}$ and with maximum characteristic size c_2 propagate in an unstable fashion.

Once Eq. (19) is satisfied by microcracks whose orientations are within a small orientation scope $0 \leqslant \theta \leqslant \theta_{cc}$ and with maximum characteristic size c_2, they will experience the secondary unstable growth, which may cause a transition from the distributed damage to the localization of damage and a rapid stress drop at the transition strain ε_{cc}. During the stage, only microcracks whose orientations are within a small orientation scope $0 \leqslant \theta \leqslant \theta_{cc}$ and with maximum characteristic size c_2 propagate further and other microcracks undergo elastic unloading. In strain-controlled tests, the deformation which has received contributions from all microcracks during the first two stages concentrates gradually to the minority of microcracks experiencing the secondary growth, which results in a localization of deformation. Therefore, the macroscopic stress drop is the result of the localization of damage and deformation.

The relation between c_3 and σ can be obtained approximately from the criterion (19), we have

$$c_3 = \frac{(v_r - 0.5v)^2 (K_{ICC}^d)^2}{\pi (v_r - v)^2 \sigma_2^2}. \tag{21}$$

The compliance tensor due to the microcracks experiencing the secondary growth can be obtained by

$$S_{ij}^{i3} = \frac{(1 - v_0^2)}{E_0} \rho \int_0^{\theta_{cc}} \int_{c_2}^{c_3} c^2 (g_{2i} g_{2j} + g_{3i} g_{3j}) p(\theta) p(c) \, \mathrm{d}c \, \mathrm{d}\theta. \tag{22}$$

The compliance tensor contributing from unstable microcracks can be evaluated as

$$S_{ij}^{i2} = \frac{(1-v_0^2)}{E_0}\rho \int_0^{\theta_{u2}} \int_{c_0}^{c_2} (g_{2i}g_{2j} + g_{3i}g_{3j}) c^2 p(c) p(\theta)\, \mathrm{d}c\, \mathrm{d}\theta + \frac{(1-v_0^2)}{E_0}\rho \int_{\theta_{u2}}^{\theta_{u3}} \int_{c_{01}}^{c_2} (g_{2i}g_{2j} + g_{3i}g_{3j}) c^2 p(c) p(\theta)\, \mathrm{d}c\, \mathrm{d}\theta, \tag{23}$$

where

$$\theta_{u3} = \arccos\left[\frac{(v_r - 0.5v)K_{IC}^d}{(v_r - v)\sigma_{2cc}\sqrt{\pi c_1}}\right]^{1/2}, \qquad \theta_{u2} = \arccos\left[\frac{(v_r - 0.5v)K_{IC}^d}{(v_r - v)\sigma_{2cc}\sqrt{\pi c_0}}\right]^{1/2}.$$

The compliance tensor attributing to stable microcracks can be computed as

$$S_{ij}^{i1} = \frac{(1-v_0^2)}{E_0}\rho \int_{\theta_{u3}}^{\frac{\pi}{2}} \int_{c_0}^{c_1} (g_{2i}g_{2j} + g_{3i}g_{3j}) c^2 p(c) p(\theta)\, \mathrm{d}c\, \mathrm{d}\theta + \frac{(1-v_0^2)}{E_0}\rho \int_{\theta_{u2}}^{\theta_{u3}} \int_{c_0}^{c_{01}} (g_{2i}g_{2j} + g_{3i}g_{3j}) c^2 p(c) p(\theta)\, \mathrm{d}c\, \mathrm{d}\theta. \tag{24}$$

During the stage, the stress–strain relation can be evaluated by

$$\varepsilon_{ij} = (S_{ij}^0 + S_{ij}^{i1} + S_{ij}^{i2} + S_{ij}^{i3})\sigma_{ij}. \tag{25}$$

During the stage of stress drop, the strain maintains constant, we have

$$\varepsilon_{2cc} = \varepsilon_2, \tag{26}$$

where ε_{2cc} is the axial strain at peak loads σ_{2cc}, ε_2 is the axial strain during stage of stress drop.

According to (26), the magnitude of the stress drop can be determined. It is assumed that the stage of rapid stress drop intersects that of tension softening at the point where the value of stress is σ_{sc}.

If $\sigma_2 < \sigma_{sc}$, that is, the stage of strain softening. During the stage of strain softening, some of the microcracks which have undergone the secondary growth will propagate further, while other microcracks will simultaneously experience unloading. Meanwhile the growth criterion (19) must be satisfied by microcracks whose orientations are within a small orientation scope $0 \leqslant \theta \leqslant \theta_{cc}$ and with maximum characteristic size c_2. The compliance tensor due to the microcracks experiencing the secondary growth, unstable microcracks and stable microcracks S_{ij}^{i3}, S_{ij}^{i2}, S_{ij}^{i1} can be evaluated by (22)–(24).

The stress–strain relation can be computed by

$$\varepsilon_{ij} = (S_{ij}^0 + S_{ij}^{i1} + S_{ij}^{i2} + S_{ij}^{i3})\sigma_{ij}. \tag{27}$$

It is assumed that all microcrack are distributed uniformly in the orientations and sizes space. The stress–strain relation for microcrack-weakened rock under dynamic uniaxial tensile loading can be expressed as (for plane strain)

$$\varepsilon_2 = \begin{cases} F_0\sigma_2 & (0 < \sigma_2 < \sigma_{2c}), \\ [F_0 + F(\theta_1)]\sigma_2 & (\sigma_{2c} < \sigma_2 < \sigma_{2cc}), \\ [F_0 + F(\theta_2)]\sigma_{2cc} & (\sigma_{sc} < \sigma_2 < \sigma_{2cc}), \\ [F_0 + F(\theta_2) + F(\theta_{cc})]\sigma_2 & (0 < \sigma_2 < \sigma_{sc}), \end{cases} \tag{28}$$

where

$$F(\theta_1) = \frac{1-v_0^2}{4\pi E_0}\rho(c_2^2 - c^2)(2\theta_1 + \sin 2\theta_1), \qquad c_3 = \frac{(v_r - 0.5v)^2 (K_{ICC}^d)^2}{(v_r - v)^2 \pi \sigma_2^2},$$

$$\theta_2 = \arccos\left(\frac{\sigma_{2c}}{\sigma_{2cc}}\right)^{1/2}, \qquad \theta_1 = \arccos\left(\frac{\sigma_{2c}}{\sigma_2}\right)^{1/2}, \qquad \sigma_{sc} = \frac{[F_0 + F(\theta_2)]\sigma_{2cc}}{[F_0 + F(\theta_2) + F(\theta_{cc})]},$$

$$F(\theta_{cc}) = \frac{1 - v_0^2}{4\pi E_0}\rho(c_3^2 - c_2^2)(2\theta_{cc} + \sin 2\theta_{cc}),$$

$$F(\theta_2) = \frac{1 - v_0^2}{4\pi E_0}\rho(c_2^2 - c^2)(2\theta_2 + \sin 2\theta_2), \qquad F_0 = \frac{1 - v_0^2}{E_0}\left(1 + \frac{1}{4}\rho c^2\right).$$

For mesoscopic heterogeneous rock, the probability density function describing the distribution of the orientations of microcracks $p(\theta)$ is approximated perfectly by Weibull distribution:

$$p(\theta) = \frac{m}{\theta_0}\left(\frac{\theta}{\theta_0}\right)^{m-1}\exp\left[-\left(\frac{\theta}{\theta_0}\right)^m\right], \tag{29}$$

where m is Weibull modulus, θ_0 is characteristic angle.

The probability density function describing the distribution of the sizes of microcracks $p(c)$ is approximated perfectly by Rayleigh function:

$$p(c) = A\left(\frac{c}{c_{00}}\right)\exp\left[-\left(\frac{c}{c_{00}}\right)^2\right], \tag{30}$$

where c_{00} is characteristic length, A is the normalization constant ($A = 2/c_{00}$).

To simplify the analysis, it is assumed that $m = 1$, the stress–strain relation for mesoscopic heterogeneous rock under dynamic uniaxial tensile loading is given as (for plane strain)

$$\varepsilon_2 = \begin{cases} F_1\sigma_2 & (0 < \sigma_2 < \sigma_{2c}), \\ (F_1 + F_2)\sigma_2 & (\sigma_{2c} < \sigma_2 < \sigma_{2cc}), \\ (F_1 + F_3)\sigma_{2cc} & (\sigma_{sc} < \sigma_2 < \sigma_{2cc}), \\ (F_1 + F_3 + F_4)\sigma_2 & (0 < \sigma_2 < \sigma_{sc}), \end{cases} \tag{31}$$

where

$$F_1 = \frac{1 - v_0^2}{E_0}\left[1 + \frac{\rho A}{1 + 4\theta_0^2}(1 + 2\theta_0^2 - 2\theta_0^2\exp(-0.5\pi/\theta_0))\right],$$

$$F_2 = \frac{(1 - v_0^2)\rho\theta_0(D + B - A)}{E_0(1 + 4\theta_0^2)}\left[\exp\left(-\frac{\theta_{u1}}{\theta_0}\right)\cos\theta_{u1}\left(2\sin\theta_{u1} - \frac{\cos\theta_{u1}}{\theta_0}\right) - 2\theta_0\exp\left(-\frac{\theta_{u1}}{\theta_0}\right)\right]$$

$$+ \frac{(1 - v_0^2)\rho\theta_0(C - B - D)}{E_0(1 + 4\theta_0^2)}\left[\exp\left(-\frac{\theta_{u0}}{\theta_0}\right)\cos\theta_{u0}\left(2\sin\theta_{u0} - \frac{\cos\theta_{u0}}{\theta_0}\right) - 2\theta_0\exp\left(-\frac{\theta_{u0}}{\theta_0}\right)\right]$$

$$+ \frac{(1 - v_0^2)\rho}{E_0(1 + 4\theta_0^2)}\left[-2A\theta_0^2\exp\left(-\frac{\pi}{2\theta_0}\right) + (1 + 2\theta_0^2)C\right],$$

$$F_3 = \frac{(1-v_0^2)\rho\theta_0(D+B-A)}{E_0(1+4\theta_0^2)}\left[\exp\left(-\frac{\theta_{u3}}{\theta_0}\right)\cos\theta_{u3}\left(2\sin\theta_{u3}-\frac{\cos\theta_{u3}}{\theta_0}\right)-2\theta_0\exp\left(-\frac{\theta_{u3}}{\theta_0}\right)\right]$$
$$+\frac{(1-v_0^2)\rho\theta_0(C-B-D)}{E_0(1+4\theta_0^2)}\left[\exp\left(-\frac{\theta_{u2}}{\theta_0}\right)\cos\theta_{u2}\left(2\sin\theta_{u0}-\frac{\cos\theta_{u2}}{\theta_0}\right)-2\theta_0\exp\left(-\frac{\theta_{u2}}{\theta_0}\right)\right]$$
$$+\frac{(1-v_0^2)\rho}{E_0(1+4\theta_0^2)}\left[-2A\theta_0^2\exp\left(-\frac{\pi}{2\theta_0}\right)+(1+2\theta_0^2)C\right],$$

$$F_4 = \frac{(1-v_0^2)\rho H}{E_0(1+4\theta_0^2)}\left[\theta_0\exp\left(-\frac{\theta_{cc}}{\theta_0}\right)\cos\theta_{cc}\left(2\sin\theta_{cc}-\frac{1}{\theta_0}\cos\theta_{cc}\right)-2\theta_0^2\exp\left(-\frac{\theta_{cc}}{\theta_0}\right)+2\theta_0^2+1\right],$$

$$A = c_0^2\exp\left[-\left(\frac{c_0}{c_{00}}\right)^2\right]+c_{00}^2\exp\left[-\left(\frac{c_0}{c_{00}}\right)^2\right]-c_1^2\exp\left[-\left(\frac{c_1}{c_{00}}\right)^2\right]-c_{00}^2\exp\left[-\left(\frac{c_1}{c_{00}}\right)^2\right],$$

$$B = c_0^2\exp\left[-\left(\frac{c_0}{c_{00}}\right)^2\right]+c_{00}^2\exp\left[-\left(\frac{c_0}{c_{00}}\right)^2\right]-c_{02}^2\exp\left[-\left(\frac{c_{02}}{c_{00}}\right)^2\right]-c_{00}^2\exp\left[-\left(\frac{c_{02}}{c_{00}}\right)^2\right],$$

$$C = c_0^2\exp\left[-\left(\frac{c_0}{c_{00}}\right)^2\right]+c_{00}^2\exp\left[-\left(\frac{c_0}{c_{00}}\right)^2\right]-c_2^2\exp\left[-\left(\frac{c_2}{c_{00}}\right)^2\right]-c_{00}^2\exp\left[-\left(\frac{c_2}{c_{00}}\right)^2\right],$$

$$D = c_{02}^2\exp\left[-\left(\frac{c_{02}}{c_{00}}\right)^2\right]+c_{00}^2\exp\left[-\left(\frac{c_{02}}{c_{00}}\right)^2\right]-c_2^2\exp\left[-\left(\frac{c_2}{c_{00}}\right)^2\right]-c_{00}^2\exp\left[-\left(\frac{c_2}{c_{00}}\right)^2\right],$$

$$H = c_2^2\exp\left[-\left(\frac{c_2}{c_{00}}\right)^2\right]+c_{00}^2\exp\left[-\left(\frac{c_2}{c_{00}}\right)^2\right]-c_3^2\exp\left[-\left(\frac{c_3}{c_{00}}\right)^2\right]-c_{00}^2\exp\left[-\left(\frac{c_3}{c_{00}}\right)^2\right],$$

$$c_{02} = \frac{(v_r-0.5v)^2(K_{IC}^d)^2}{\pi(v_r-v)^2\sigma_2^2(\theta_{u1}-\theta_{u0})}\left(\frac{\sin\theta_{u1}}{3\cos^3\theta_{u1}}+\frac{2\sin\theta_{u1}}{3\cos\theta_{u1}}-\frac{\sin\theta_{u0}}{3\cos^3\theta_{u0}}-\frac{2\sin\theta_{u0}}{3\cos\theta_{u0}}\right),$$

$$\sigma_{sc} = \frac{(F_1+F_3)\sigma_{2cc}}{F_1+F_3+F_4}, \qquad c_3 = \frac{(v_r-0.5v)^2(K_{ICC}^d)^2}{\pi(v_r-v)^2\sigma_2^2}.$$

For $m > 1$, the stress–strain relation for mesoscopic heterogeneous rock under dynamic uniaxial tensile loading can be obtained similarly as Eq. (31).

It should be mentioned that the constitutive relations (28) and (31) are obtained without taking into account interaction between microcracks. Such an assumption is an acceptable approximation for most stages of rock material before a macrocrack initiates, even though localization of damage occurs in the stage of tension softening because only a minority of microcracks experience secondary growth. If interaction between microcracks is considered, the constitutive relation will become more complicated. In our

modelling, we have assumed the initial flaws to be two-dimensional slit cracks, however, one can extend the present model to three-dimensional penny-shaped cracks and, of course, the results will become better.

3. Comparison with experimental results

In order to illustrate the four stages of the stress–strain relation predicted by the theoretical model, we selected experimental results obtained by Okubo and Fukui (1996) for Inada rock specimens subjected to uniaxial tensile loading. The magnitude of stress drop is 5.6 MPa, the drops occurred gradually over 130 s in the experiment, thus stress rate is 4.3×10^{-2} s^{-1}. The stress rate of 4.3×10^{-2} s^{-1} is in the dynamic regime. The Inada rock is a relatively homogeneous and nearly brittle, compact rock whose properties and mechanical behavior are thoroughly known in rock mechanics. Since the crack growth length is less than 25 cm in 130 s, the crack growth velocity $v = \mathrm{d}l/\mathrm{d}t$ is less than 0.1 m/s. As the velocity of the Rayleigh wave for the granite is about 2000 m/s, the crack growth velocity v is small and the effect on dynamic SIF under the dynamic regime can be neglected. The function $k(v)$ can then be regarded as one.

The following material parameters were used in computations for Inada rock:

$$E_0 = 37,600 \text{ MPa}, \quad c = 7.5\times10^{-4} \text{ m}, \quad c_2 = 5\times10^{-3} \text{ m}, \quad K_{\mathrm{IC}}^{\mathrm{d}} = 0.1 \text{ MPa}\sqrt{\text{m}},$$
$$v_0 = 0.23, \quad \sigma_{2cc} = -6.7 \text{ MPa}, \quad \rho = 4.5\times10^{5}, \quad \theta_{cc} = 0.1^0, \quad K_{\mathrm{ICC}}^{\mathrm{d}} = 0.85 \text{ MPa}\sqrt{\text{m}},$$
$$p(\theta) = 1/\pi. \tag{32}$$

In (32), the numerical values of E_0, v_0, σ_{2cc} were read off from the tests by Okubo and Fukui (1996). ρ, c, c_2 were estimated by SEM observations, $K_{\mathrm{IC}}^{\mathrm{d}}$, $K_{\mathrm{ICC}}^{\mathrm{d}}$ were estimated by the three-point bend tests. The solid curves depicted in Fig. 2 represent the stress–strain relation predicted by the present model, while dots are the experimental results measured by Okubo and Fukui (1996). It can be seen in Fig. 2 that the agreement between theoretical and experimental results is fair good. Note that the material parameters (32) used in the computations are realistic and documented in the referenced literature typically of micromechanical models, the present formulation does not contain no fitting parameters. All the involved parameters have clear physical meaning.

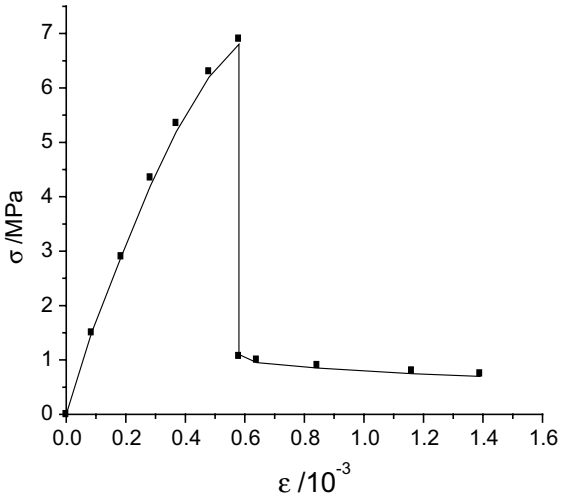

Fig. 2. The present model vs testing result for Inada rock.

4. Sensitivity study of mechanical parameters toward stress–strain relation

4.1. Sensitivity study of fracture toughness K^d_{ICC} toward stress–strain relation

The solid curves 1, 2, 3 and 4 depicted in Fig. 3 represent the stress–strain relation predicted by the present model, when fracture toughness $K^{\mathrm{d}}_{\mathrm{ICC}}$ is 0.65, 0.85, 1.0 and 1.25 MPa$\sqrt{\mathrm{m}}$, respectively. It can be seen in Fig. 3 that the magnitude of the stress drop is larger as well as the strength for microcrack-weakened rock, as fracture toughness $K^{\mathrm{d}}_{\mathrm{ICC}}$ is larger. It is obvious that fracture toughness $K^{\mathrm{d}}_{\mathrm{ICC}}$ will mainly influence the strength for microcrack-weakened rock.

4.2. Sensitivity study of the initial microcrack density parameter ρ toward stress–strain relation

The solid curves 1, 2, 3 and 4 depicted in Fig. 4 represent the stress–strain relation predicted by the present model, when the initial microcrack density parameter ρ is 2.25×10^5, 4.5×10^5, 9×10^5 and 1.8×10^6, respectively. It can be observed in Fig. 4 that strain is larger, as the initial microcrack density parameter ρ is larger. It shows that the initial microcrack density parameter ρ will not affect the strength for microcrack-weakened rock when the crack interaction effects are ignored.

4.3. Sensitivity study of the microcrack half-length c, c_2 toward stress–strain relation

The solid curves 1, 2, 3 and 4 plotted in Fig. 5 represent the stress–strain relation predicted by the present model, when the microcrack half-length c, c_2 are 7×10^{-4} and 4.5×10^{-3} m, 7.5×10^{-4} and 5×10^{-3} m, 8×10^{-4} and 6×10^{-3} m, 9×10^{-4} and 7×10^{-3} m, respectively. It can be seen in Fig. 5 that strain is larger as the microcrack half-length c, c_2 are larger, but the strength for microcrack-weakened rock will decrease as the microcrack half-length c, c_2 become larger. It is evident that influence of the microcrack half-length c, c_2 on the deformation and strength for microcrack-weakened rock are obvious.

4.4. Sensitivity study of the crack growth velocity v toward stress–strain relation

The solid curves 1, 2, 3 and 4 plotted in Fig. 6 represent the stress–strain relation predicted by the present model, while the crack growth velocity v is 0, 100, 500 and 1000 m/s, respectively. It can be observed in

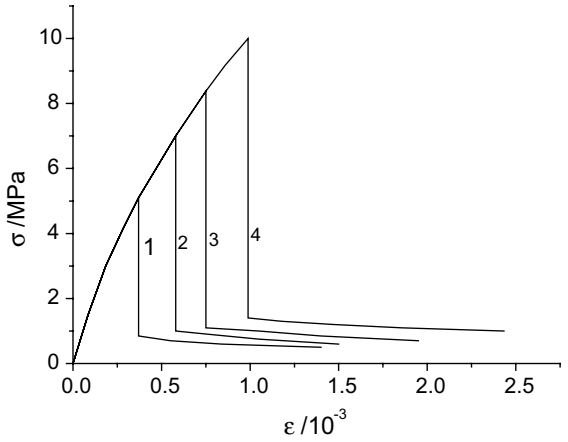

Fig. 3. Sensitivity of fracture toughness $K^{\mathrm{d}}_{\mathrm{ICC}}$ toward stress–strain relation.

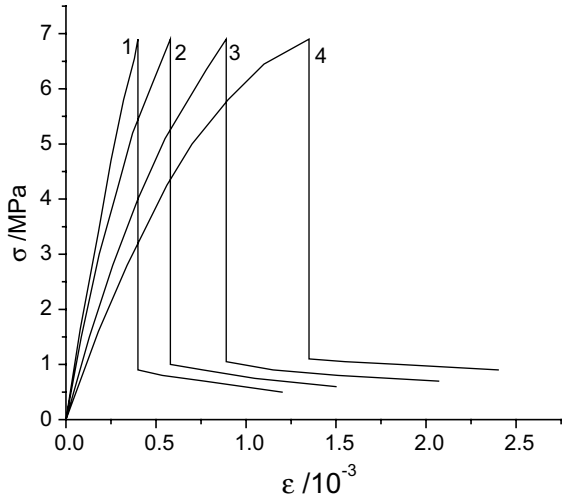

Fig. 4. Sensitivity of the initial microcrack density parameter ρ toward stress–strain relation.

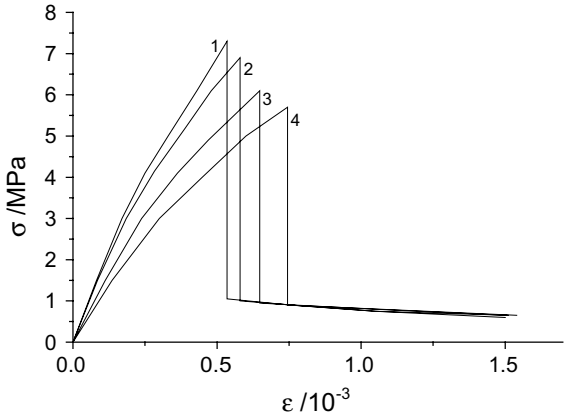

Fig. 5. Sensitivity of the microcrack half-length c, c_2 toward stress–strain relation.

Fig. 6 that the magnitude of the stress drop is smaller and time of stress drop is shortened as the crack growth velocity v become larger. It is shown that the crack growth velocity v mainly affects the magnitude of the stress drop and time of stress drop.

4.5. Sensitivity study of the crack growth velocity v combined with fracture toughness K^d_{ICC} toward stress–strain relation

The solid curves 1, 2, 3 and 4 plotted in Fig. 7 represent the stress–strain relation predicted by the present model, while the crack growth velocity v and fracture toughness $K^{\mathrm{d}}_{\mathrm{ICC}}$ is 0 and 0.65 MPa$\sqrt{\mathrm{m}}$, 100 m/s and 0.85 MPa$\sqrt{\mathrm{m}}$, 500 m/s and 1.0 MPa$\sqrt{\mathrm{m}}$, and 1000 m/s and 1.25 MPa$\sqrt{\mathrm{m}}$, respectively. It can be seen in Fig. 7 that the residual strength of microcrack-weakened rock is higher as the crack growth velocity v and fracture toughness $K^{\mathrm{d}}_{\mathrm{ICC}}$ are larger.

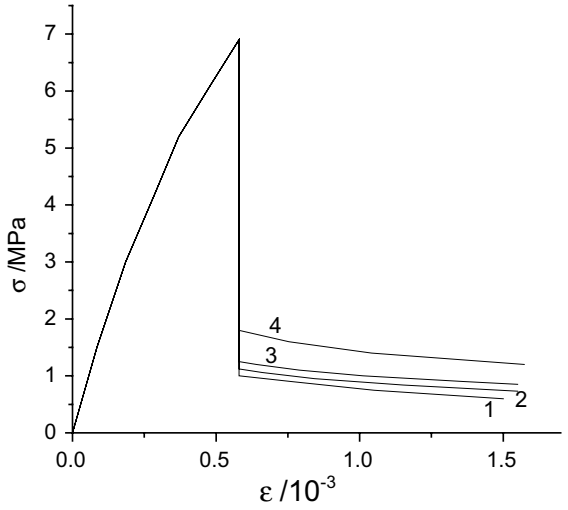

Fig. 6. Sensitivity of the crack growth velocity v toward stress–strain relation.

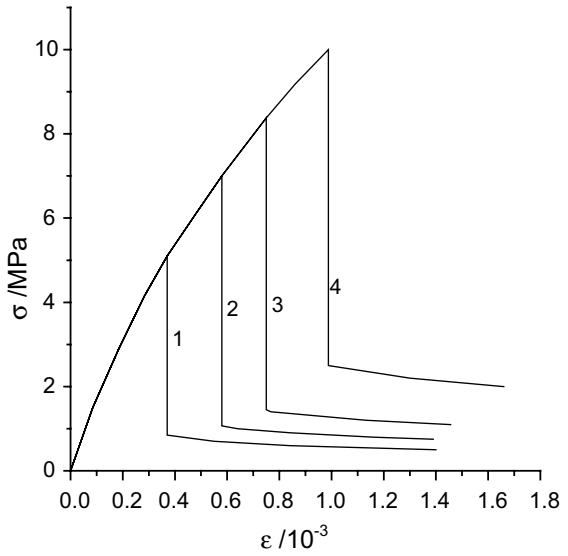

Fig. 7. Sensitivity of the crack growth velocity v combined with fracture toughness $K_{\mathrm{ICC}}^{\mathrm{d}}$ toward stress–strain relation.

5. Sensitivity study of the crack growth velocity toward the strength of microcrack-weakened rock

The solid curve plotted in Fig. 8 represents the strength of microcrack-weakened rock predicted by the present model, while the crack growth velocity v is in the range 0–1500 m/s. It is obvious in Fig. 8 that the strength of microcrack-weakened rock is higher as the crack growth velocity v is larger if $K_{\mathrm{ICC}}^{\mathrm{d}}$ remains constant. This is in agreement with results obtained later (Jin, 2001).

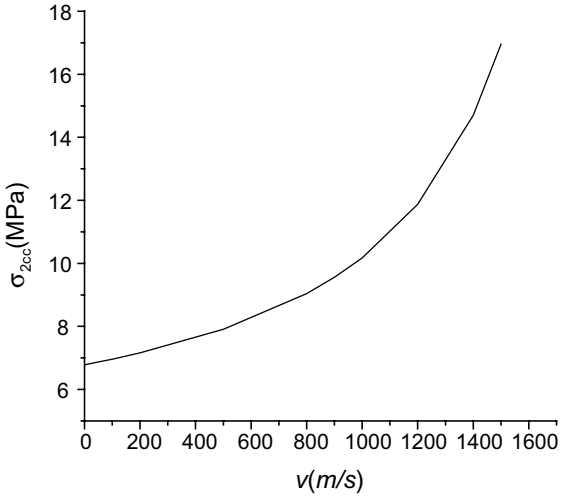

Fig. 8. Sensitivity of the crack growth velocity v toward the strength of crack-weakened rock for fracture toughness $K_{ICC}^{d} = 0.85$, the microcrack half-length $c_2 = 5 \times 10^{-3}$ m, the initial microcrack density parameter $\rho = 4.5 \times 10^5$.

6. Conclusions

Based on the micromechanics, the localization of deformation is analyzed and the complete stress–strain relation for mesoscopic heterogeneous rock under dynamic uniaxial tensile loading is investigated. The main points are briefly summarized as follows:

(1) The deformation for mesoscopic heterogeneous rock under dynamic uniaxial tensile loading can be splitted into the deformation due to an undamaged matrix, the stable microcracks, the unstable microcracks propagating in a stable fashion, and the microcracks experiencing the secondary growth.
(2) The stress–strain relation for mesoscopic heterogeneous rock under dynamic uniaxial tensile loading include four stages, that is, the stage of linear elasticity, prepeak nonlinear hardening, stress drop and strain softening. It is different from the conventional model that localization of damage and deformation are introduced into the constitutive relation. The reasons causing localization of damage and deformation are discussed.
(3) The influence of all microcracks with different sizes and orientations are introduced into the constitutive relation by using the probability density function describing the distribution of orientations $p(\theta)$ and the probability density function describing the distribution of sizes $p(c)$. The influence of Weibull distribution describing the distribution of orientations $p(\theta)$ and Rayleigh function describing the distribution of sizes $p(c)$ on the constitutive relation are researched.
(4) The validity of theoretical model is verified by experimental results.
(5) It can be seen from sensitivity study of mechanical parameters toward stress–strain relation that fracture toughness K_{ICC}^{d} will mainly influence the strength for microcrack-weakened rock, influence of the initial microcrack density parameter ρ on the deformation for microcrack-weakened rock is important, the microcrack half-length c, c_2 will mainly affect the strength and deformation for microcrack-weakened rock, effect of the crack growth velocity v on the magnitude of the stress drop and time of stress drop is obvious, the crack growth velocity v combined with fracture toughness K_{ICC}^{d} mainly influences the residual strength of microcrack-weakened rock.

(6) The crack growth velocity v evidently affects the strength of microcrack-weakened rock, the strength of microcrack-weakened rock is higher as the crack growth velocity v is larger.
(7) One can extend the present model to three-dimensional penny-shaped cracks.

Acknowledgements

The author thank Prof. Charles R. Steele for helpful discussions. This work was supported by the National Science Foundation of China (No. 59879012, 59649008).

References

Blanton, T.L., 1981. Effect of strain rate from 10^{-2} to 10 s^{-1} in triaxial compression tests on three rocks. Int. J. Rock Mech. Min. Sci. 18, 47–62.

Chong, K.P., Hoy, P.M., Smith, J.M., Paulsen, B.Y., 1980. Effects of strain rate on oil shale fracturing. Int. J. Rock Mech. Min. Sci. 17, 35–43.

Freund, L.B., 1973. Crack propagation in an elastic solid subjected to general loading. J. Mech. Phys. Solids 21, 47–61.

Freund, L.B., 1990. Dynamic Fracture Mechanics. Cambridge University Press, Cambridge.

Jin, F., 2001. The Non-linear Rheological Behavior of Rock. Hehai University Press, China.

Okubo, S., Fukui, K., 1996. Complete stress–strain curves for various rock types in uniaxial tension. Int. J. Rock Mech. Min. Sci. 35, 549–556.

Okubo, S., Jin, F., Akiyama, M., 1993. Loading-rate dependency of uniaxial and indirect tensile strength. J. Mining Mater. Process. Instit. Japan 109, 865–869.

Sumarac, D., Krajcinovic, D.A., 1987. Self-consistent model for microcrack-weakened solids. Mech. Mater. 6, 39–52.

Zhou, X.P., in press. Analysis of the localization of deformation and study on the complete stress–strain relation for mesoscopic heterogeneous rock under uniaxial tensile loading. Applied Mathematics and Mechanics.